

ScoreAdv: Score-based Targeted Generation of Natural Adversarial Examples via Diffusion Models

Chihan Huang^{1,*}, Hao Tang^{2,†}

¹Nanjing University of Science and Technology

²Peking University

huangchihan@njust.edu.cn, haotang@pku.edu.cn

Abstract

Despite the success of deep learning across various domains, it remains vulnerable to adversarial attacks. Although many existing adversarial attack methods achieve high success rates, they typically rely on ℓ_p -norm perturbation constraints, which do not align with human perceptual capabilities. Consequently, researchers have shifted their focus toward generating natural, unrestricted adversarial examples (UAEs). GAN-based approaches suffer from inherent limitations, such as poor image quality due to instability and mode collapse. Meanwhile, diffusion models have been employed for UAE generation, but they still rely on iterative PGD perturbation injection, without fully leveraging their central denoising capabilities. In this paper, we introduce a novel approach for generating UAEs based on diffusion models, named ScoreAdv. This method incorporates an interpretable adversarial guidance mechanism to gradually shift the sampling distribution towards the adversarial distribution, while using an interpretable saliency map to inject the visual information of a reference image into the generated samples. Notably, our method is capable of generating an unlimited number of natural adversarial examples and can attack not only classification models but also retrieval models. We conduct extensive experiments on ImageNet and CelebA datasets, validating the performance of ScoreAdv across ten target models in both black-box and white-box settings. Our results demonstrate that ScoreAdv achieves state-of-the-art attack success rates and image quality. Furthermore, the dynamic balance between denoising and adversarial perturbation enables ScoreAdv to remain robust even under defensive measures.

Code — <https://github.com/6tonystark6/ScoreAdv>

Introduction

Recent years have witnessed the remarkable application of deep learning in various domains, including image classification (Cheng, Yap, and Wen 2023), autonomous driving (Feng et al. 2023), medical image analysis (Zhang, Xie, and Chen 2023), etc. However, studies such as (Szegedy et al. 2014) have demonstrated that deep learning models are

highly susceptible to adversarial examples—subtle, imperceptible perturbations that mislead models into wrong predictions with high confidence (Huang and Shen 2025). The transferability of adversarial examples poses an even greater security risk, as adversarial samples crafted for one target model can be effectively transferred to different models, potentially compromising the security of multiple systems.

Many previous adversarial attacks have been based on ℓ_p -norm constraints (Dong et al. 2019; Zhao et al. 2024) to bound perturbation strength. However, recent research (Zhao, Liu, and Larson 2020) has shown that ℓ_p -norm poorly aligns with human perceptual similarity. As shown in Figure 1, attacks based on ℓ_p -norm, despite having a small ℓ_∞ value, are more easily noticeable to the human eye.

In contrast to attacks based on ℓ_p -norm perturbations, this paper investigates unrestricted adversarial example generation, where the generated samples are not constrained by any norm limitations, but instead optimize the input noise vector directly. Such perturbations typically exhibit large-scale, semantically coherent patterns that enhance attack success rates while remaining imperceptible (Jia et al. 2022).

The concept of UAE was first introduced by Song et al. (Song et al. 2018), who employed a generative adversarial network (GAN) with an auxiliary classifier to directly generate adversarial samples. However, GAN-based methods suffer from instability, mode collapse, and limited interpretability, often resulting in lower-quality outputs. In contrast, diffusion models (Ho, Jain, and Abbeel 2020) offer more stable training, better image quality, and broader distribution coverage (Dhariwal and Nichol 2021), making them more suitable for generating natural adversarial images.

The iterative denoising process in diffusion models naturally serves as a robust mechanism, capable of mitigating adversarial noise while retaining attack efficacy. (Dhariwal and Nichol 2021) also highlighted that conditions can be incorporated into the denoising process to guide the generation. This characteristic enables us to carefully introduce adversarial information during the denoising process, thus achieving the generation of natural adversarial samples. However, existing diffusion-based attack methods have not fully exploited this capability. They often rely on PGD-based perturbations at each step (Chen et al. 2023a,b), or lack reference-image conditioning (Dai, Liang, and Xiao 2025), limiting image quality and the full use of diffusion’s potential.

*Work Done during the visit at Peking University.

†Corresponding author.

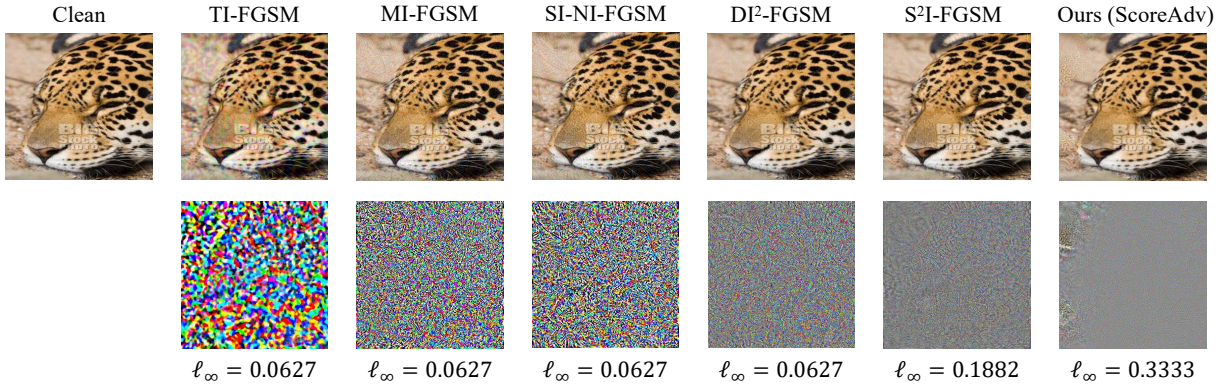


Figure 1: Adversarial attack results generated by various attack methods. The second row illustrates the difference between the benign and adversarial images. For detailed examination, please enlarge the image.

In this paper, we propose a novel and interpretable UAE generation method based on diffusion models, called ScoreAdv. Compared to previous diffusion-based adversarial attack methods, ScoreAdv **1)** introduces an interpretable adversarial perturbation method at each diffusion step, gradually shifting the sampling distribution towards the adversarial distribution. **2)** Proposes using ScoreCAM to highlight the salient regions of a reference image, enabling the generation of adversarial examples that are consistent with the reference image. **3)** Iteratively optimizes the initial sampling noise to incorporate both the target semantic information and the visual features of the reference image, improving the adversarial sample’s alignment with the intended objectives.

Our contributions can be summarized as follows:

1. We propose ScoreAdv, a training-free, unrestricted adversarial example generation framework based on diffusion models. ScoreAdv can generate an unlimited number of natural adversarial examples, targeting not only classification but also recognition models.
2. We introduce an interpretable perturbation mechanism at each diffusion step to guide sampling, and incorporate interpretable saliency-based visual information from an optional reference image to improve semantic relevance.
3. Comprehensive experiments on ten target models demonstrate that ScoreAdv outperforms existing methods in both black-box and white-box settings, achieving superior attack success and visual quality. The dynamic interplay between denoising and adversarial perturbation also improves robustness against defenses.

Related Work

Adversarial Attacks

Adversarial attacks are commonly classified as white-box or black-box, depending on the attacker’s knowledge of the target model. White-box attacks assume full access to model architecture, gradients, and parameters, with representative methods including FGSM (Goodfellow, Shlens, and Szegedy 2015), PGD (Madry et al. 2018a), and DeepFool (Moosavi-Dezfooli, Fawzi, and Frossard 2016). In contrast, black-box attacks, which only rely on input-output

queries, are more challenging and better reflect real-world conditions. Notable examples include ZOO (Chen et al. 2017) and DeepSearch (Zhang, Chowdhury, and Christakis 2020). Attacks can also be untargeted, aiming to misclassify into any incorrect label, or targeted, forcing misclassification into a specific class, often posing greater threats. Many black-box attacks leverage transferability (Papernot, McDaniel, and Goodfellow 2016; Dong et al. 2018), applying white-box techniques on surrogate models to generate transferable adversarial examples.

Unrestricted Adversarial Attacks

Due to the inadequacy of ℓ_p -norm in capturing perceptual similarity in RGB space, researchers have increasingly explored unrestricted adversarial attacks. Early works, such as (Zhao, Dua, and Singh 2018), modified GAN latent codes via auxiliary classifiers, but suffered from limited image quality. (Bhattad et al. 2019) perturbed color and texture, while (Yuan et al. 2022) used a color distribution library and a neighborhood search to improve realism. (Jia et al. 2022) generated attribute-based adversarial noise targeting facial features. More recent methods leverage diffusion models for unrestricted attacks. (Dai, Liang, and Xiao 2025) introduced adversarial guidance for stable generation; (Chen et al. 2023a) proposed AdvDiffuser, injecting PGD perturbations during sampling; and (Chen et al. 2025) employed latent-space mapping with content-preserving structures and attention-based distractions to craft adversarial examples.

Diffusion Models

Diffusion models are based on stochastic processes and Markov chains, with a forward process of gradually adding noise and a reverse denoising process. Given an image \mathbf{x}_0 , the forward process adds noise over T steps using a schedule $\beta_{1:T}$, generating an increasing noisy image sequence.

$$q(\mathbf{x}_t|\mathbf{x}_{t-1}) = \mathcal{N}\left(\sqrt{1-\beta_t}\mathbf{x}_{t-1}, \beta_t\mathbf{I}\right). \quad (1)$$

In the denoising process, the diffusion model learns to predict and remove noise, effectively restoring \mathbf{x}_T back to its original form \mathbf{x}_0 .

$$p_\theta(\mathbf{x}_{t-1}|\mathbf{x}_t) = \mathcal{N}(\mu_\theta(\mathbf{x}_t, t), \Sigma_\theta(\mathbf{x}_t, t)), \quad (2)$$

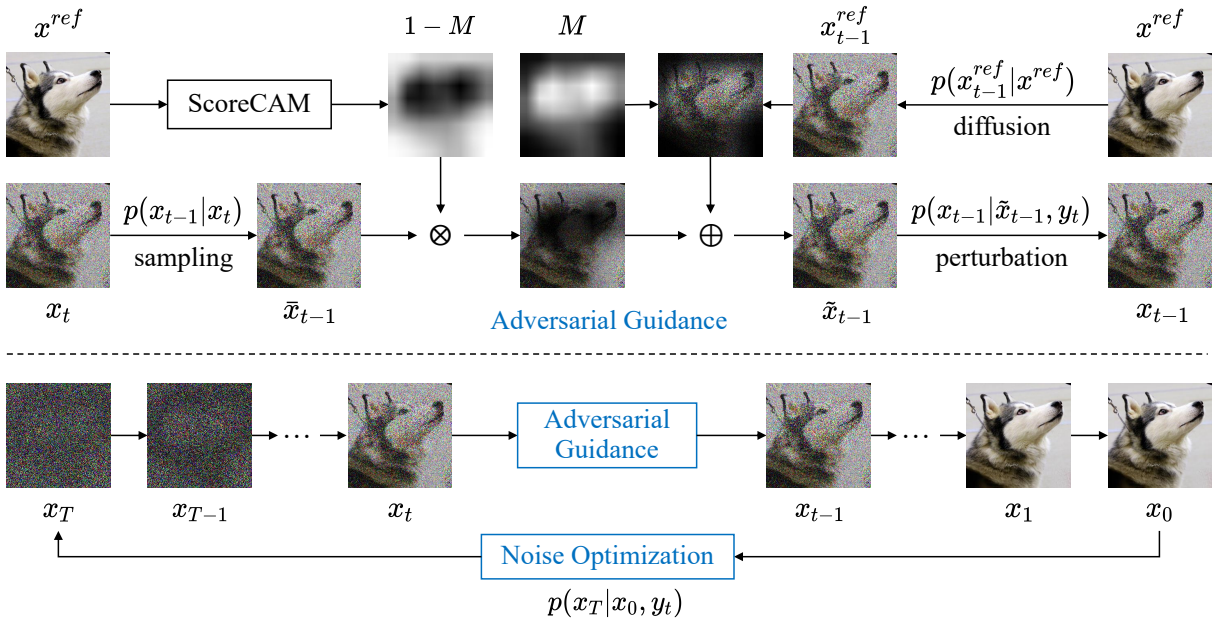


Figure 2: Overall framework of our ScoreAdv to generate adversarial images. The lower part illustrates the trained diffusion model. In each diffusion step, we employ adversarial guidance by first sampling \tilde{x}_{t-1} using the diffusion model. Subsequently, adversarial perturbation is introduced based on the gradient derived from the target label and target model. If the content information from a reference image is required, we utilize ScoreCAM to generate its saliency map. We use the diffusion process to obtain x_{t-1}^{ref} , which is then weighted and combined with \tilde{x}_{t-1} to produce the input for the next diffusion step x_{t-1} .

where $\mu_\theta(\mathbf{x}_t, t) = \frac{1}{\sqrt{\alpha_t}} \left(\mathbf{x}_t - \frac{\beta_t}{\sqrt{1-\alpha_t}} \epsilon_\theta(\mathbf{x}_t, t) \right)$, for simplification, $\alpha = 1 - \beta$, $\bar{\alpha}_t = \prod_{i=1}^t \alpha_i$, $\bar{\beta}_t = \frac{1-\bar{\alpha}_{t-1}}{1-\bar{\alpha}_t} \beta_t$.

Subsequent advances include Improved DDPM (Nichol and Dhariwal 2021), which learns a variance schedule to improve sampling quality and efficiency. (Dhariwal and Nichol 2021) introduced conditional diffusion, incorporating the gradient of cross-entropy loss from a target model into the sampling mean for class-conditioned generation.

$$p_{\theta, \phi}(\mathbf{x}_{t-1} | \mathbf{x}_t, y) = \mathcal{N}(\mu_\theta(\mathbf{x}_t) + \Sigma_\theta \nabla_{\mathbf{x}_t} \log p_\phi(y | \mathbf{x}_t), \Sigma_\theta). \quad (3)$$

Furthermore, classifier-free guidance (Ho and Salimans 2021) enables the incorporation of class information without the need for an additional trained classifier.

$$\tilde{\epsilon}_t = (1 + s_c) \epsilon_\theta(\mathbf{x}_t, y) - s_c \epsilon_\theta(\mathbf{x}_t). \quad (4)$$

Methodology

Formulation

Instead of adding perturbations to clean samples, we aim to leverage a generative model to produce UAEs (Song et al. 2018), yielding more natural adversarial inputs. Given a generative model \mathcal{G} , a target model f , ground truth label y , target label y_{tar} , and an optional reference image x^{ref} , the generated UAE is defined as:

$$A_{UAE} \triangleq \{ \mathbf{x}_{adv} \in \mathcal{G}(z_{adv}, y, \mathbf{x}^{ref}) | f(\mathbf{x}_{adv}) = y_{tar} \}. \quad (5)$$

The overall framework of the proposed ScoreAdv is shown in Figure 2. In this paper, we focus on targeted at-

tacks, where the goal is to generate a sample with true label y that the target model misclassifies as a specified label y_{tar} .

Adversarial Perturbation

When using a pre-trained diffusion model, the denoising process gradually transforms noise into a natural image. Inspired by (Dhariwal and Nichol 2021), we found that during the denoising process, the gradient $\nabla_{\mathbf{x}_t} \log p_\phi(y | \mathbf{x}_t)$ can be used to guide the shift of the sampling distribution. Our objective is to generate an image \mathbf{x}_0 with a pre-trained diffusion model $\epsilon_\theta(\mathbf{x}_t, y)$, which appears consistent with the target label y , but is misclassified by the target model as $y_{tar} \neq y$. We achieve this through adversarial perturbations.

First, based on classifier-free guidance, we can use a pre-trained diffusion model to obtain the sampling formula guided by the ground truth label y as the target class.

$$\tilde{\mathbf{x}}_{t-1} = \frac{1}{\sqrt{\alpha_t}} \left(\mathbf{x}_t - \frac{1-\alpha_t}{\sqrt{1-\bar{\alpha}_t}} \tilde{\epsilon}_t \right) + \sigma_t z_t, \quad (6)$$

where ϵ_θ represents the pre-trained diffusion model, s_c is the classifier guidance scale, $\tilde{\epsilon}_t$ is the predicted noise obtained using classifier-free guidance following (4), z_t is random noise, and $\tilde{\mathbf{x}}_{t-1}$ is the image sampled with the true label y , incorporating class information.

Next, we aim to sample a sample near $\tilde{\mathbf{x}}_{t-1}$ that embodies the semantic information of the target class y_{tar} :

$$p(\tilde{\mathbf{x}}_{t-1} | \tilde{\mathbf{x}}_{t-1}, f(\tilde{\mathbf{x}}_{t-1}) = y_{tar}). \quad (7)$$

This sampling process is similar to that of conditional diffusion models. We can use the gradient information of $\tilde{\mathbf{x}}_{t-1}$

Algorithm 1: ScoreAdv Diffusion Sampling

Input: Ground truth label y , (optional) reference image \mathbf{x}^{ref} , target label y_{tar} or target image \mathbf{x}_{tar} , target model f , pretrained diffusion model ϵ_θ , reverse generation process timestep T , noise optimization times N , adversarial guidance scale s_a , classifier guidance scale s_c , noise optimization guidance scale s_n , noise schedule $\beta_{1:T}$;

Output: Adversarial image \mathbf{x}_{adv} ;

```

1:  $\mathbf{x}_T \sim \mathcal{N}(0, \mathbf{I})$ ,  $\mathbf{x}_{adv} = \{\}$ ;
2: for all  $i = 1, \dots, N$  do
3:   for all  $t = T, \dots, 1$  do
4:      $\tilde{\epsilon}_t = (1 + s_c) \epsilon_\theta(\mathbf{x}_t, y) - s_c \epsilon_\theta(\mathbf{x}_t)$ ;
5:      $\bar{\mathbf{x}}_{t-1} = \frac{1}{\sqrt{\alpha_t}} \left( \mathbf{x}_t - \frac{1-\alpha_t}{\sqrt{1-\alpha_t}} \tilde{\epsilon}_t \right) + \sigma_t z_t$ ;
6:     if  $\mathbf{x}^{ref}$  then
7:        $\mathbf{m} = \text{ScoreCAM}(\mathbf{x}^{ref}, f, y)$ ;
8:        $\mathbf{x}_{t-1}^{ref} \sim \mathcal{N}(\sqrt{\alpha_{t-1}} \mathbf{x}^{ref}, (1 - \alpha_{t-1}) \mathbf{I})$ ;
9:        $\mathbf{x}_{t-1} = \bar{\mathbf{x}}_{t-1} \odot (1 - \mathbf{m}) + \mathbf{x}_{t-1}^{ref} \odot \mathbf{m}$ ;
10:    end if
11:     $\hat{\mathbf{x}}_0 = \frac{1}{\sqrt{\alpha_t}} (\bar{\mathbf{x}}_{t-1} - \sqrt{1 - \alpha_t} \cdot \tilde{\epsilon}_{t-1})$ ;
12:     $\mathbf{g} = \nabla_{\mathbf{x}_{t-1}} \log p_f(y_{tar} | \bar{\mathbf{x}}_{t-1})$ ;           if  $y_{tar}$ 
13:     $\mathbf{g} = \nabla_{\hat{\mathbf{x}}_0} \log p_f(\mathbf{x}_{tar} | \hat{\mathbf{x}}_0)$ ;           if not  $y_{tar}$ 
14:     $\tilde{\mathbf{x}}_{t-1} = \bar{\mathbf{x}}_{t-1} + \sigma_t^2 s_a \mathbf{g}$ ;
15:  end for
16:   $\mathbf{g}_n = \nabla_{\mathbf{x}_0} \log p_f(y_{tar} | \mathbf{x}_0)$ ;           if  $\mathbf{x}^{ref}$ 
17:   $\mathbf{g}_n = \nabla_{\mathbf{x}_0} \log p_f(\mathbf{x}_{tar} | \mathbf{x}_0)$ ;           if not  $\mathbf{x}^{ref}$ 
18:   $\mathbf{x}_T \leftarrow \mathbf{x}_T + \bar{\sigma}_T^2 s_n \mathbf{g}_n$ ;
19:  if  $f(\mathbf{x}_0) = y_{tar}$  then
20:     $\mathbf{x}_{adv} \leftarrow \mathbf{x}_0$ ;
21:  end if
22: end for

```

from the target model to guide this sampling.

$$\tilde{\mathbf{x}}_{t-1} = \bar{\mathbf{x}}_{t-1} + \sigma_t^2 s_a \nabla_{\bar{\mathbf{x}}_{t-1}} \log p_f(y_{tar} | \bar{\mathbf{x}}_{t-1}), \quad (8)$$

where s_a represents the adversarial guidance scale.

The derivation of Equation (8) is provided in Supplementary Material. Intuitively, a small perturbation is introduced to shift $\bar{\mathbf{x}}_{t-1}$ toward the target class y_{tar} , increasing the likelihood that the generated sample $\tilde{\mathbf{x}}_{t-1}$ is classified as y_{tar} .

Image Recognition. While the above adversarial perturbation targets classification tasks, our method also extends to image recognition. Given a target image \mathbf{x}_{tar} and a similarity model $f(\cdot, \cdot)$, we apply the same procedure to obtain $\bar{\mathbf{x}}_{t-1}$, and then sample $\tilde{\mathbf{x}}_{t-1}$ as follows:

$$\begin{aligned} \tilde{\mathbf{x}}_{t-1} &= \bar{\mathbf{x}}_{t-1} + \sigma_t^2 s_a \nabla_{\hat{\mathbf{x}}_0} \log p_f(\mathbf{x}_{tar} | \hat{\mathbf{x}}_0), \\ \hat{\mathbf{x}}_0 &= \frac{1}{\sqrt{\alpha_t}} (\bar{\mathbf{x}}_{t-1} - \sqrt{1 - \alpha_t} \cdot \tilde{\epsilon}_{t-1}), \end{aligned} \quad (9)$$

where $\hat{\mathbf{x}}_0$ is the predicted clean image from $\bar{\mathbf{x}}_{t-1}$, and $\tilde{\epsilon}_{t-1}$ is the predicted noise at step $t-1$. We measure similarity between \mathbf{x}_{tar} and $\hat{\mathbf{x}}_0$ rather than $\bar{\mathbf{x}}_{t-1}$, since the latter contains significant noise. As the target model is trained on clean images, evaluating on denoised predictions better reflects its behavior. Thus, we first predict $\hat{\mathbf{x}}_0$ from $\bar{\mathbf{x}}_{t-1}$, then measure $f(\mathbf{x}_{tar} | \hat{\mathbf{x}}_0)$.

ScoreCAM-based Inpainting

We introduce ScoreCAM to guide the diffusion denoising process with a reference image, generating natural adversarial examples that resemble it. Unlike gradient-based methods such as GradCAM (Selvaraju et al. 2017), which suffer from vanishing gradients and instability (Wang et al. 2020), ScoreCAM avoids gradient dependence.

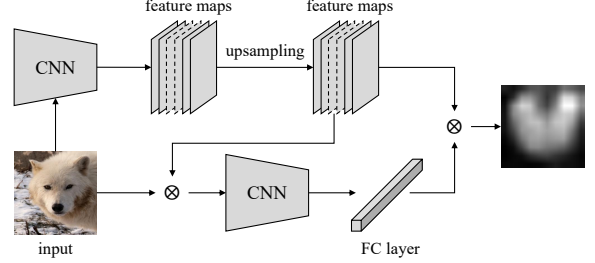


Figure 3: Illustration of ScoreCAM.

As shown in Figure 6, given an image X and model f with layer l , we extract activation maps A_l^k for each channel k and assign weights based on the score increase S , yielding a more stable and interpretable saliency map.

$$S(A_l^k) = f(X \odot s(\text{Up}(A_l^k))), \quad (10)$$

where $\text{Up}(\cdot)$ represents the upsampling function, which up-scales A_l^k to the size of input X , and $s(x) = \frac{x - \min x}{\max x - \min x}$ is the normalization function that maps x to $[0, 1]$.

Thus, for a given class c , ScoreCAM can be computed as:

$$\begin{aligned} \text{ScoreCAM}^c &= \text{ReLU} \left(\sum_k \alpha_k^c A_l^k \right), \\ \alpha_k^c &= \frac{\exp(S^c(A_l^k))}{\sum_j \exp(S^c(A_l^j))}, \end{aligned} \quad (11)$$

where $S^c(\cdot)$ represents the logits corresponding to class c .

Thus, given the reference image \mathbf{x}^{ref} , target model f and ground truth label y , we can obtain the saliency map \mathbf{m} .

$$\mathbf{m} = \text{ScoreCAM}(\mathbf{x}^{ref}, f, y). \quad (12)$$

At each diffusion step t , we gradually inject information from the reference image \mathbf{x}^{ref} into $\bar{\mathbf{x}}_t$ by applying the forward diffusion process to obtain the noisy version \mathbf{x}_{t-1}^{ref} .

$$\mathbf{x}_{t-1}^{ref} \sim \mathcal{N} \left(\sqrt{\alpha_{t-1}} \mathbf{x}^{ref}, (1 - \alpha_{t-1}) \mathbf{I} \right). \quad (13)$$

We leverage the concept of image inpainting (Lugmayr et al. 2022) to perform a weighted fusion of \mathbf{x}_{t-1}^{ref} with $\tilde{\mathbf{x}}_t$.

$$\mathbf{x}_{t-1} = \tilde{\mathbf{x}}_{t-1} \odot (1 - \mathbf{m}) + \mathbf{x}_{t-1}^{ref} \odot \mathbf{m}. \quad (14)$$

Noise Optimization

(Zhou et al. 2025) show that certain noise types yield better results. Motivated by this, we incorporate prior information about the target label into the initial noise. Specifically, after

Table 1: Attack performance comparison of various methods on the ImageNet dataset. We report ASR (%) and transferability. S. represents the surrogate model, while T. represents the target model. In cases where the surrogate model and the target model are identical, the scenario is classified as a white-box attack, with the background highlighted in gray for clarity. Avg. represents the average ASR of black-box attacks. The best result is **bolded** and the second best result is underlined.

S.	T.	Attacks	CNNs					Transformers			MLPs		Avg.↑
			Res50	VGG19	Inc-v3	WRN50	CNX	ViT-B	Swin-B	DeiT-B	Mix-B	Mix-L	
Res-50		PGD	94.4	27.6	30.0	15.7	12.3	13.3	22.1	18.0	41.4	33.9	23.81
		DI2-FGSM	91.0	23.3	22.5	25.6	12.7	9.9	14.4	11.2	42.1	40.0	22.41
		S2I-FGSM	<u>95.7</u>	29.5	31.9	28.6	17.9	16.1	23.8	15.8	45.8	44.3	28.19
		cAdv	92.5	45.0	30.0	25.7	19.3	20.3	27.8	21.0	51.4	49.9	32.27
		NCF	91.4	46.7	38.8	34.7	24.9	24.4	26.8	27.3	55.2	53.0	36.87
		AdvDiffuser	91.4	50.9	43.3	39.2	40.8	37.5	46.7	42.0	56.4	53.8	45.62
		DiffAttack	87.0	51.2	42.1	40.7	41.0	35.9	45.0	41.1	58.0	55.3	45.59
		Advdiff	92.1	<u>53.0</u>	47.2	<u>44.5</u>	<u>46.7</u>	40.4	<u>46.8</u>	<u>45.8</u>	<u>62.4</u>	<u>60.1</u>	<u>49.66</u>
		ScoreAdv	97.6	57.0	<u>46.7</u>	48.9	46.9	<u>40.1</u>	47.0	46.2	65.3	62.7	51.20
	VGG19		PGD	20.6	97.5	24.9	18.2	19.0	11.5	16.9	13.3	33.3	29.1
		DI2-FGSM	23.0	<u>98.2</u>	29.5	24.6	24.1	13.4	22.5	14.2	39.8	34.3	25.04
		S2I-FGSM	30.1	100.0	35.6	26.1	31.5	17.0	26.7	21.4	45.3	41.2	30.54
		cAdv	36.5	90.2	39.2	30.7	22.7	25.2	36.0	24.7	45.4	44.8	33.91
		NCF	36.8	90.8	41.1	30.3	25.1	26.6	37.7	29.5	49.4	46.1	35.84
		AdvDiffuser	40.7	94.0	46.2	38.4	36.2	28.6	34.4	30.1	58.9	51.6	40.57
		DiffAttack	<u>42.0</u>	93.4	45.3	38.0	30.0	28.5	35.7	30.5	55.6	48.2	39.31
		Advdiff	41.8	94.7	<u>48.5</u>	<u>40.1</u>	<u>37.4</u>	35.4	<u>39.5</u>	<u>36.0</u>	<u>60.3</u>	<u>54.4</u>	<u>43.71</u>
		ScoreAdv	48.7	100.0	49.1	47.2	39.1	<u>32.9</u>	41.6	39.1	85.7	75.0	50.93
Inc-v3			PGD	21.3	23.6	94.2	15.3	14.7	13.2	15.9	15.2	26.5	24.1
		DI2-FGSM	20.0	28.5	90.2	14.3	15.1	13.8	19.5	14.6	31.1	26.5	20.38
		S2I-FGSM	24.1	32.2	93.1	25.7	27.1	19.8	25.3	21.2	39.2	35.4	27.78
		cAdv	31.7	38.6	83.3	27.2	26.2	29.6	34.2	30.7	43.5	42.6	33.81
		NCF	35.5	39.3	86.3	31.7	28.9	31.9	33.9	33.3	44.7	41.9	35.68
		AdvDiffuser	39.4	45.8	89.1	36.6	34.6	34.4	40.2	37.6	53.1	50.8	41.39
		DiffAttack	40.1	46.4	88.5	35.5	34.8	35.3	41.3	38.1	50.7	48.7	41.21
		Advdiff	42.9	<u>47.6</u>	91.4	<u>39.3</u>	<u>36.7</u>	<u>39.9</u>	<u>44.2</u>	<u>41.8</u>	<u>54.5</u>	<u>52.3</u>	<u>44.36</u>
		ScoreAdv	<u>40.6</u>	67.2	<u>93.4</u>	39.9	40.8	39.4	45.1	43.6	72.9	58.5	49.78
	ViT-B		PGD	25.6	28.0	26.6	19.7	18.7	86.4	28.7	22.5	29.0	26.2
		DI2-FGSM	24.9	35.0	30.6	26.5	22.8	89.8	31.0	28.2	33.1	30.9	29.22
		S2I-FGSM	29.2	38.5	35.9	27.6	29.4	90.3	34.5	31.0	41.7	38.2	34.00
		cAdv	33.6	42.0	39.0	30.3	28.2	85.8	35.9	32.4	45.6	41.2	36.47
		NCF	40.6	44.9	43.1	33.8	33.3	81.0	38.7	35.7	51.1	46.5	40.86
		AdvDiffuser	46.2	47.8	49.0	44.1	39.7	87.6	42.4	40.1	54.6	51.4	46.14
		DiffAttack	45.4	49.7	48.6	<u>44.3</u>	38.5	86.0	41.2	38.8	55.1	52.6	46.02
		Advdiff	<u>50.6</u>	<u>53.2</u>	<u>52.0</u>	46.4	43.7	<u>90.1</u>	<u>47.1</u>	<u>44.3</u>	<u>58.7</u>	<u>56.9</u>	<u>50.32</u>
		ScoreAdv	54.2	57.3	53.2	42.8	<u>42.0</u>	88.7	57.9	59.0	85.2	64.5	57.34

generating \mathbf{x}_0 , we apply diffusion process and use gradient signals from the target model to guide noise optimization.

$$\mathbf{x}_T = (\sqrt{\bar{\alpha}_t}\mathbf{x}_0 + \sqrt{1 - \bar{\alpha}_t}\epsilon) + \bar{\sigma}_T^2 s_a \nabla_{\mathbf{x}_0} \log p_f(y_{tar}|\mathbf{x}_0), \quad (15)$$

where $\epsilon \sim \mathcal{N}(0, \mathbf{I})$, the former represents the forward diffusion process, while the latter denotes the gradient of \mathbf{x}_0 with respect to the target model.

For image recognition models, the equation for noise optimization is similar to the one described above:

$$\mathbf{x}_T = (\sqrt{\bar{\alpha}_t}\mathbf{x}_0 + \sqrt{1 - \bar{\alpha}_t}\epsilon) + \bar{\sigma}_T^2 s_a \nabla_{\mathbf{x}_0} \log p_f(\mathbf{x}_{tar}|\mathbf{x}_0). \quad (16)$$

ScoreAdv Algorithm

Algorithm 1 summarizes the ScoreAdv pipeline. At each diffusion step, we sample $\tilde{\mathbf{x}}_{t-1}$ using classifier-free guidance, then apply adversarial guidance to obtain $\hat{\mathbf{x}}_{t-1}$. If a reference image \mathbf{x}^{ref} is available, we use ScoreCAM to inject content information. After denoising for \mathbf{x}_0 , noise optimization is performed, and the process is repeated for N cycles.

Experiments

Datasets

For image classification, we use 1,000 samples from the ImageNet validation set, covering 1,000 categories. Images are

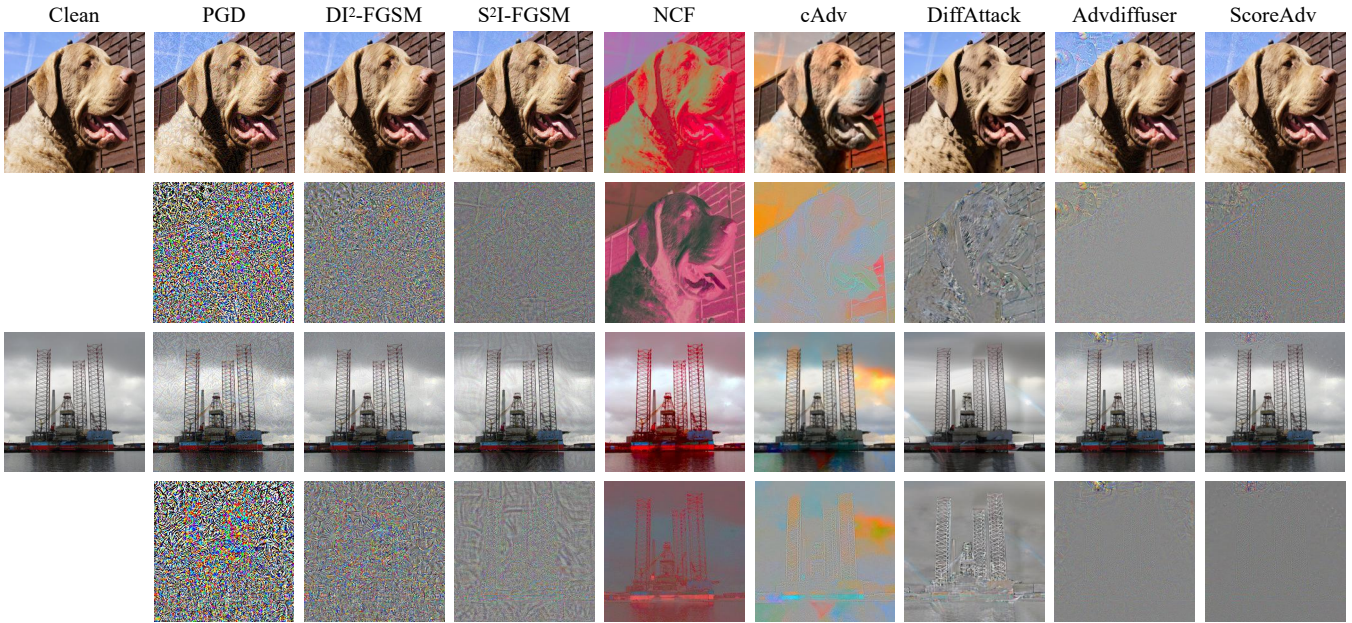


Figure 4: Visualization of adversarial images and perturbations generated by different attack methods. The upper row displays the adversarial images, while the lower row illustrates the corresponding perturbations.

resized to 224×224 to match the diffusion model.

For face recognition, we conduct experiments on CelebA and LFW. CelebA contains 202,599 images across 10,177 identities, and LFW includes 13,233 images of 5,749 individuals. We randomly select 1,000 images for evaluation.

Experiment Settings

We utilize the pre-trained Guided Diffusion model from OpenAI (Dhariwal and Nichol 2021), avoiding training from scratch. We select a diffusion step as $T = 1000$, noise optimization iterations as $N = 3$, adversarial guidance scale as $s_a = 0.3$, and noise optimization scale as $s_n = 0.8$.

We evaluate attacks on models from three architecture families. CNN-based models include ResNet (Res50) (He et al. 2016), VGG19 (Simonyan and Zisserman 2015), Inception-v3 (Szegedy et al. 2016), WideResNet50-2 (WRN50) (Zagoruyko and Komodakis 2016), and ConvNeXt (CNX) (Liu et al. 2022). Transformers models include ViT-B/16 (ViT-B) (Kolesnikov et al. 2021), Swin Transformer (Swin-B) (Liu et al. 2021), and DeiT-B (Touvron et al. 2020). MLP-based models include Mixer-B/16 (Mix-B) and Mixer-L/16 (Mixer-L) (Tolstikhin et al. 2021).

We use attack success rate (ASR) to measure attack effectiveness. To assess imperceptibility and visual quality, we report FID (Heusel et al. 2017), LPIPS (Zhang et al. 2018), PSNR, and SSIM (Horé and Ziou 2010).

Results

Targeted Attack Performance. Table 1 reports the ASR on ImageNet. ScoreAdv achieves SOTA performance in most scenarios, outperforming methods such as PGD (Madry et al. 2018b), DI^2 -FGSM (Xie et al. 2019), S^2I -FGSM (Long et al. 2022), cAdv (Bhattad et al. 2019), NCF (Yuan et al.

Table 2: Image quality comparison of various methods on ImageNet dataset. The best result is **bolded** and the second best result is underlined.

Attacks	FID↓	LPIPS↓	PSNR↑	SSIM↑
PGD	72.740	0.276	23.867	0.6541
DI^2 -FGSM	71.650	0.198	26.388	0.7599
S^2I -FGSM	51.022	0.158	29.808	0.8296
cAdv	69.593	0.246	24.113	0.7059
NCF	70.857	0.355	14.994	0.6087
DiffAttack	48.639	0.169	27.450	0.6546
AdvDiffuser	<u>45.399</u>	<u>0.137</u>	<u>30.146</u>	<u>0.8302</u>
ScoreAdv	44.932	0.124	30.817	0.8319

2022), AdvDiffuser (Chen et al. 2023a), DiffAttack (Chen et al. 2025), and Advdiff (Dai, Liang, and Xiao 2025).

While ScoreAdv may slightly underperform in isolated cases, these methods often yield lower-quality adversarial examples with poor black-box transferability. Additional results on recognition models are provided in Supplementary Material, and ScoreAdv performs even better in this setting.

Generation Quality. ScoreAdv consistently produces the most natural and coherent adversarial images. In Figure 6, it best preserves perceptual fidelity and captures high-frequency details, enhancing its realism. Table 2 presents the quantitative comparison of image quality. ScoreAdv achieves the lowest FID, indicating better preservation of the reference image distribution. Higher PSNR and SSIM reflect minimal, well-placed perturbations, while lower LPIPS confirms better alignment with human perception.

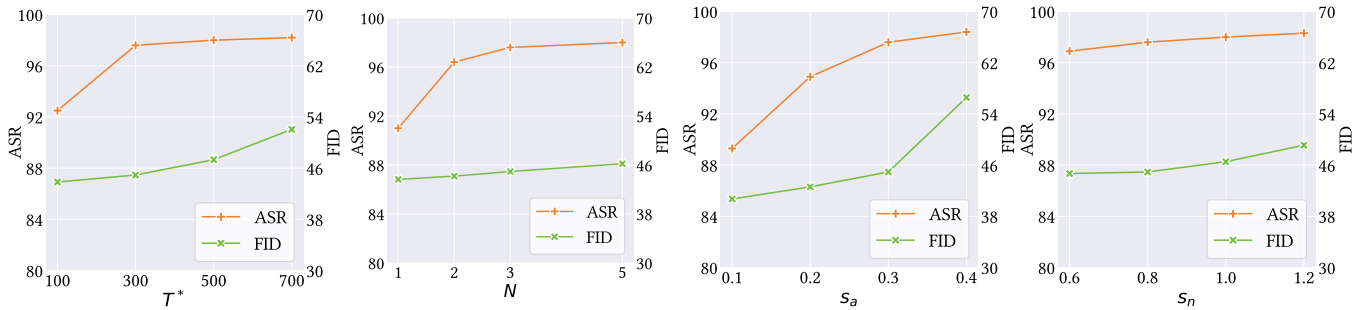


Figure 5: Ablation analysis of ScoreAdv parameters. We selected ResNet-50 as the target model and employed ASR and FID as the evaluation metrics to assess the attack effectiveness and generated image quality, respectively.

Table 3: Attack robustness comparison of various methods against different defense strategies. For SR, NRP, and DiffPure, we present the reduction in ASR following their application. The best result is **bolded** and the second best result is underlined.

	AdvProp	R&P	RandS	Bit-Red	Adv-Inc-v3	IncRes-v2 _{ens}	Inc-v3	SR	NRP	Diffpure
PGD	59.5	15.9	36.7	17.3	30.8	19.0	94.2	-26.1	-49.6	-51.2
DI2-FGSM	56.7	20.6	33.4	19.0	25.7	12.8	90.2	-34.2	-37.0	-45.7
S2I-FGSM	75.2	22.7	54.9	21.8	41.0	28.0	93.1	-13.3	-25.2	-31.6
cAdv	75.6	19.4	48.5	19.3	38.7	26.2	83.3	-38.0	-30.4	-43.3
NCF	78.2	19.1	50.6	17.5	42.5	27.8	86.3	-21.5	-27.8	-33.8
AdvDiffuser	74.9	20.8	53.5	22.9	46.2	32.9	89.1	-25.0	-29.6	-33.4
DiffAttack	76.5	24.5	54.8	23.7	44.8	31.6	88.5	-32.9	-42.2	-34.1
Advdiff	<u>81.0</u>	<u>49.1</u>	<u>71.2</u>	<u>44.4</u>	<u>56.1</u>	<u>44.9</u>	91.4	-18.4	-28.6	<u>-20.4</u>
ScoreAdv	83.6	52.4	73.8	46.3	57.6	48.1	<u>93.4</u>	<u>-17.6</u>	<u>-25.3</u>	-18.7

Robustness Against Defense Methods. To evaluate the robustness of ScoreAdv, we conducted a series of adversarial defense experiments. Specifically, AdvProp (Xie et al. 2020), R&P (Xie et al. 2018), RandS (Cohen, Rosenfeld, and Kolter 2019), Bit-Red (Xu, Evans, and Qi 2018), Adv-Inc-v3 (Kurakin et al. 2018b), and IncRes-v2_{ens} (Kurakin et al. 2018a) apply defense mechanisms or train robust models before attack. SR (Mustafa et al. 2020), NRP (Naseer et al. 2020), and DiffPure (Nie et al. 2022) operate by purifying images post-attack to mitigate adversarial effects.

As shown in Table 3, ScoreAdv demonstrates superior robustness compared to previous methods and exhibits slightly better robustness than AdvDiff. This enhanced performance may be attributed to both methods that utilize the inherent distribution-shifting property of diffusion models. Moreover, the dynamic interplay of iterative denoising and adversarial perturbation injection within inadvertently contributes to improving the robustness of the generated images.

Parameter Analysis

In Figure 5, we conduct a comprehensive parameter analysis on diffusion steps T^* , noise optimization times N , adversarial guidance scale s_a , and noise optimization scale s_n .

Noise Addition Steps T^* . T^* denotes the number of diffusion steps where adversarial perturbations are applied, specifically during the final T^* steps. As shown, increasing T^* improves ASR but may degrade image quality due to accumulated noise. Our T^* balances ASR and visual fidelity.

Noise Optimization Times N . A larger N enables further optimization of the initial noise, improving adversarial effectiveness and ASR, similar to increasing iterations in GANs. However, excessive N may distort the noise too much, degrading image quality. As shown in the figure, a small N already yields high ASR, so we choose a moderate value to balance performance and visual fidelity.

Adversarial Guidance Scale s_a And Noise Optimization Scale s_n . In the figure, increasing s_a improves attack performance by amplifying perturbation strength and enhancing guidance toward the target class. However, overly large s_a degrades image quality. The effect of s_n follows a similar trend but has less impact, as it only applies when $N > 1$.

Please see supplementary material for additional experiments on more SOTA methods and ensemble attacks and ablation studies on saliency maps.

Conclusion

In this paper, we propose ScoreAdv, an interpretable method for generating natural UAEs by leveraging the distribution shift in diffusion models. It uses a pretrained diffusion model with adversarial guidance injected during denoising, and integrates ScoreCAM to incorporate visual cues from a reference image. Experiments show that ScoreAdv achieves SOTA performance in both black-box and white-box attacks on classification and recognition tasks, while maintaining high image quality and strong robustness against defenses.

References

- Bhattach, A.; Chong, M. J.; Liang, K.; Li, B.; and Forsyth, D. A. 2019. Unrestricted Adversarial Examples via Semantic Manipulation. In *International Conference on Learning Representations*.
- Chattopadhyay, A.; Sarkar, A.; Howlader, P.; and Balasubramanian, V. N. 2018. Grad-CAM++: Improved Visual Explanations for Deep Convolutional Networks. In *2018 IEEE Winter Conference on Applications of Computer Vision (WACV)*.
- Chen, J.; Chen, H.; Chen, K.; Zhang, Y.; Zou, Z.; and Shi, Z. 2025. Diffusion Models for Imperceptible and Transferable Adversarial Attack. *IEEE Transactions on Pattern Analysis and Machine Intelligence*, 47(2): 961–977.
- Chen, P.-Y.; Zhang, H.; Sharma, Y.; Yi, J.; and Hsieh, C.-J. 2017. ZOO: Zeroth Order Optimization Based Black-box Attacks to Deep Neural Networks without Training Substitute Models. In *Proceedings of the 10th ACM Workshop on Artificial Intelligence and Security, AISec '17*, 15–26. New York, NY, USA: Association for Computing Machinery. ISBN 9781450352024.
- Chen, S.; Liu, Y.; Gao, X.; and Han, Z. 2018. MobileFaceNets: Efficient CNNs for Accurate Real-Time Face Verification on Mobile Devices. In *Biometric Recognition*.
- Chen, X.; Gao, X.; Zhao, J.; Ye, K.; and Xu, C.-Z. 2023a. AdvDiffuser: Natural Adversarial Example Synthesis with Diffusion Models. In *2023 IEEE/CVF International Conference on Computer Vision (ICCV)*, 4539–4549.
- Chen, Z.; Li, B.; Wu, S.; Jiang, K.; Ding, S.; and Zhang, W. 2023b. Content-based Unrestricted Adversarial Attack. In Oh, A.; Naumann, T.; Globerson, A.; Saenko, K.; Hardt, M.; and Levine, S., eds., *Advances in Neural Information Processing Systems*, volume 36, 51719–51733. Curran Associates, Inc.
- Cheng, H.; Yap, K.-H.; and Wen, B. 2023. Reconciliation of statistical and spatial sparsity for robust visual classification. *Neurocomputing*, 529: 140–151.
- Cohen, J.; Rosenfeld, E.; and Kolter, Z. 2019. Certified Adversarial Robustness via Randomized Smoothing. In Chaudhuri, K.; and Salakhutdinov, R., eds., *Proceedings of the 36th International Conference on Machine Learning*, volume 97 of *Proceedings of Machine Learning Research*, 1310–1320. PMLR.
- Collins, M.; Vice, J.; French, T.; and Mian, A. 2025. NatADiff: Adversarial Boundary Guidance for Natural Adversarial Diffusion. arXiv:2505.20934.
- Dai, X.; Liang, K.; and Xiao, B. 2025. AdvDiff: Generating Unrestricted Adversarial Examples Using Diffusion Models. In *Computer Vision – ECCV 2024*, 93–109.
- Dhariwal, P.; and Nichol, A. 2021. Diffusion models beat GANs on image synthesis. In *Proceedings of the 35th International Conference on Neural Information Processing Systems, NIPS '21*. Red Hook, NY, USA: Curran Associates Inc. ISBN 9781713845393.
- Dong, Y.; Liao, F.; Pang, T.; Su, H.; Zhu, J.; Hu, X.; and Li, J. 2018. Boosting Adversarial Attacks with Momentum. In *2018 IEEE/CVF Conference on Computer Vision and Pattern Recognition*, 9185–9193.
- Dong, Y.; Pang, T.; Su, H.; and Zhu, J. 2019. Evading Defenses to Transferable Adversarial Examples by Translation-Invariant Attacks. In *2019 IEEE/CVF Conference on Computer Vision and Pattern Recognition (CVPR)*, 4307–4316.
- Feng, S.; Sun, H.; Yan, X.; Zhu, H.; Zou, Z.; Shen, S.; and Liu, H. 2023. Dense reinforcement learning for safety validation of autonomous vehicles. *Nature*, 615: 620–627.
- Goodfellow, I.; Shlens, J.; and Szegedy, C. 2015. Explaining and Harnessing Adversarial Examples. In *International Conference on Learning Representations*.
- He, K.; Zhang, X.; Ren, S.; and Sun, J. 2016. Deep Residual Learning for Image Recognition. In *2016 IEEE Conference on Computer Vision and Pattern Recognition (CVPR)*, 770–778.
- Heusel, M.; Ramsauer, H.; Unterthiner, T.; Nessler, B.; and Hochreiter, S. 2017. GANs trained by a two time-scale update rule converge to a local nash equilibrium. In *Proceedings of the 31st International Conference on Neural Information Processing Systems, NIPS'17*, 6629–6640. Red Hook, NY, USA: Curran Associates Inc. ISBN 9781510860964.
- Ho, J.; Jain, A.; and Abbeel, P. 2020. Denoising diffusion probabilistic models. In *Proceedings of the 34th International Conference on Neural Information Processing Systems, NIPS '20*. Red Hook, NY, USA: Curran Associates Inc. ISBN 9781713829546.
- Ho, J.; and Salimans, T. 2021. Classifier-Free Diffusion Guidance. In *NeurIPS 2021 Workshop on Deep Generative Models and Downstream Applications*.
- Horé, A.; and Ziou, D. 2010. Image Quality Metrics: PSNR vs. SSIM. In *2010 20th International Conference on Pattern Recognition*, 2366–2369.
- Huang, C.; and Shen, X. 2025. HUANG: A Robust Diffusion Model-based Targeted Adversarial Attack Against Deep Hashing Retrieval. *Proceedings of the AAAI Conference on Artificial Intelligence*, 39(4): 3626–3634.
- Jia, S.; Yin, B.; Yao, T.; Ding, S.; Shen, C.; Yang, X.; and Ma, C. 2022. Adv-Attribute: Inconspicuous and Transferable Adversarial Attack on Face Recognition. In Koyejo, S.; Mohamed, S.; Agarwal, A.; Belgrave, D.; Cho, K.; and Oh, A., eds., *Advances in Neural Information Processing Systems*, volume 35, 34136–34147. Curran Associates, Inc.
- Kolesnikov, A.; Dosovitskiy, A.; Weissenborn, D.; Heigold, G.; Uszkoreit, J.; Beyer, L.; Minderer, M.; Dehghani, M.; Houtsby, N.; Gelly, S.; Unterthiner, T.; and Zhai, X. 2021. An Image is Worth 16x16 Words: Transformers for Image Recognition at Scale.
- Kurakin, A.; Boneh, D.; Er, F. T.; Goodfellow, I.; Papernot, N.; and McDaniel, P. 2018a. Ensemble Adversarial Training: Attacks and Defenses.
- Kurakin, A.; Goodfellow, I.; Bengio, S.; Dong, Y.; Liao, F.; Liang, M.; Pang, T.; Zhu, J.; Hu, X.; Xie, C.; Wang, J.; Zhang, Z.; Ren, Z.; Yuille, A.; Huang, S.; Zhao, Y.; Zhao, Y.; Han, Z.; Long, J.; Berdibekov, Y.; Akiba, T.; Tokui, S.; and

- Abe, M. 2018b. Adversarial Attacks and Defences Competition. In *The NIPS '17 Competition: Building Intelligent Systems*, 195–231.
- Kuurila-Zhang, H.; Chen, H.; and Zhao, G. 2025. VENOM: Text-driven Unrestricted Adversarial Example Generation with Diffusion Models. arXiv:2501.07922.
- Li, J.; He, Z.; Luo, A.; Hu, J.-F.; Wang, Z. J.; and Kang, X. 2024. AdvAD: Exploring Non-Parametric Diffusion for Imperceptible Adversarial Attacks. In Globerson, A.; Mackey, L.; Belgrave, D.; Fan, A.; Paquet, U.; Tomczak, J.; and Zhang, C., eds., *Advances in Neural Information Processing Systems*, volume 37, 52323–52353. Curran Associates, Inc.
- Liu, Z.; Lin, Y.; Cao, Y.; Hu, H.; Wei, Y.; Zhang, Z.; Lin, S.; and Guo, B. 2021. Swin Transformer: Hierarchical Vision Transformer using Shifted Windows. In *2021 IEEE/CVF International Conference on Computer Vision (ICCV)*, 9992–10002.
- Liu, Z.; Mao, H.; Wu, C.-Y.; Feichtenhofer, C.; Darrell, T.; and Xie, S. 2022. A ConvNet for the 2020s. In *2022 IEEE/CVF Conference on Computer Vision and Pattern Recognition (CVPR)*, 11966–11976.
- Long, Y.; Zhang, Q.; Zeng, B.; Gao, L.; Liu, X.; Zhang, J.; and Song, J. 2022. Frequency Domain Model Augmentation for Adversarial Attack. In *Computer Vision – ECCV 2022*, 549–566. Cham: Springer Nature Switzerland. ISBN 978-3-031-19772-7.
- Lugmayr, A.; Danelljan, M.; Romero, A.; Yu, F.; Timofte, R.; and Van Gool, L. 2022. RePaint: Inpainting using Denoising Diffusion Probabilistic Models. In *2022 IEEE/CVF Conference on Computer Vision and Pattern Recognition (CVPR)*, 11451–11461.
- Madry, A.; Makelov, A.; Schmidt, L.; Tsipras, D.; and Vladu, A. 2018a. Towards Deep Learning Models Resistant to Adversarial Attacks. In *International Conference on Learning Representations*.
- Madry, A.; Makelov, A.; Schmidt, L.; Tsipras, D.; and Vladu, A. 2018b. Towards Deep Learning Models Resistant to Adversarial Attacks.
- Moosavi-Dezfooli, S.-M.; Fawzi, A.; and Frossard, P. 2016. DeepFool: A Simple and Accurate Method to Fool Deep Neural Networks. In *2016 IEEE Conference on Computer Vision and Pattern Recognition (CVPR)*, 2574–2582.
- Mustafa, A.; Khan, S. H.; Hayat, M.; Shen, J.; and Shao, L. 2020. Image Super-Resolution as a Defense Against Adversarial Attacks. *Trans. Img. Proc.*, 29: 1711–1724.
- Naseer, M.; Khan, S.; Hayat, M.; Khan, F. S.; and Porikli, F. 2020. A Self-supervised Approach for Adversarial Robustness. In *2020 IEEE/CVF Conference on Computer Vision and Pattern Recognition (CVPR)*, 259–268.
- Nichol, A. Q.; and Dhariwal, P. 2021. Improved Denoising Diffusion Probabilistic Models. In Meila, M.; and Zhang, T., eds., *Proceedings of the 38th International Conference on Machine Learning*, volume 139 of *Proceedings of Machine Learning Research*, 8162–8171. PMLR.
- Nie, W.; Guo, B.; Huang, Y.; Xiao, C.; Vahdat, A.; and Anandkumar, A. 2022. Diffusion Models for Adversarial Purification. In Chaudhuri, K.; Jegelka, S.; Song, L.; Szepesvari, C.; Niu, G.; and Sabato, S., eds., *Proceedings of the 39th International Conference on Machine Learning*, volume 162 of *Proceedings of Machine Learning Research*, 16805–16827. PMLR.
- Papernot, N.; McDaniel, P.; and Goodfellow, I. 2016. Transferability in Machine Learning: from Phenomena to Black-Box Attacks using Adversarial Samples. arXiv:1605.07277.
- Parkhi, O. M.; Vedaldi, A.; and Zisserman, A. 2015. Deep Face Recognition. In *British Machine Vision Conference*.
- Schroff, F.; Kalenichenko, D.; and Philbin, J. 2015. FaceNet: A unified embedding for face recognition and clustering. In *2015 IEEE Conference on Computer Vision and Pattern Recognition (CVPR)*, 815–823.
- Selvaraju, R. R.; Cogswell, M.; Das, A.; Vedantam, R.; Parikh, D.; and Batra, D. 2017. Grad-CAM: Visual Explanations from Deep Networks via Gradient-Based Localization. In *2017 IEEE International Conference on Computer Vision (ICCV)*, 618–626.
- Simonyan, K.; and Zisserman, A. 2015. Very Deep Convolutional Networks for Large-Scale Image Recognition. arXiv:1409.1556.
- Song, Y.; Shu, R.; Kushman, N.; and Ermon, S. 2018. Constructing Unrestricted Adversarial Examples with Generative Models. In *Advances in Neural Information Processing Systems*, volume 31. Curran Associates, Inc.
- Szegedy, C.; Vanhoucke, V.; Ioffe, S.; Shlens, J.; and Wojna, Z. 2016. Rethinking the Inception Architecture for Computer Vision. In *2016 IEEE Conference on Computer Vision and Pattern Recognition (CVPR)*, 2818–2826.
- Szegedy, C.; Zaremba, W.; Sutskever, I.; Bruna, J.; Erhan, D.; Goodfellow, I.; and Fergus, R. 2014. Intriguing properties of neural networks. In *International Conference on Learning Representations*.
- Tolstikhin, I.; Houlsby, N.; Kolesnikov, A.; Beyer, L.; Zhai, X.; Unterthiner, T.; Yung, J.; Steiner, A.; Keysers, D.; Uszkoreit, J.; Lucic, M.; and Dosovitskiy, A. 2021. MLP-mixer: an all-MLP architecture for vision. In *Proceedings of the 35th International Conference on Neural Information Processing Systems, NIPS '21*. Red Hook, NY, USA: Curran Associates Inc. ISBN 9781713845393.
- Touvron, H.; Cord, M.; Douze, M.; Massa, F.; Sablayrolles, A.; and J'egou, H. 2020. Training data-efficient image transformers & distillation through attention. In *International Conference on Machine Learning*.
- Wang, H.; Wang, Z.; Du, M.; Yang, F.; Zhang, Z.; Ding, S.; Mardziel, P.; and Hu, X. 2020. Score-CAM: Score-Weighted Visual Explanations for Convolutional Neural Networks. In *2020 IEEE/CVF Conference on Computer Vision and Pattern Recognition Workshops (CVPRW)*, 111–119.
- Wang, K.; He, X.; Wang, W.; and Wang, X. 2024. Boosting Adversarial Transferability by Block Shuffle and Rotation. In *Proceedings of the IEEE/CVF Conference on Computer Vision and Pattern Recognition (CVPR)*, 24336–24346.

- Wang, X.; and He, K. 2021. Enhancing the Transferability of Adversarial Attacks Through Variance Tuning. In *Proceedings of the IEEE/CVF Conference on Computer Vision and Pattern Recognition (CVPR)*, 1924–1933.
- Wang, X.; Zhang, Z.; and Zhang, J. 2023. Structure Invariant Transformation for better Adversarial Transferability. In *2023 IEEE/CVF International Conference on Computer Vision (ICCV)*, 4584–4596.
- Xie, C.; Tan, M.; Gong, B.; Wang, J.; Yuille, A. L.; and Le, Q. V. 2020. Adversarial Examples Improve Image Recognition. In *2020 IEEE/CVF Conference on Computer Vision and Pattern Recognition (CVPR)*, 816–825.
- Xie, C.; Wang, J.; Zhang, Z.; Ren, Z.; and Yuille, A. 2018. Mitigating Adversarial Effects Through Randomization.
- Xie, C.; Zhang, Z.; Zhou, Y.; Bai, S.; Wang, J.; Ren, Z.; and Yuille, A. L. 2019. Improving Transferability of Adversarial Examples With Input Diversity. In *Computer Vision and Pattern Recognition*, 2725–2734.
- Xu, W.; Evans, D.; and Qi, Y. 2018. Feature Squeezing: Detecting Adversarial Examples in Deep Neural Networks. In *Proceedings 2018 Network and Distributed System Security Symposium*. Internet Society.
- Yuan, S.; Zhang, Q.; Gao, L.; Cheng, Y.; and Song, J. 2022. Natural Color Fool: Towards Boosting Black-box Unrestricted Attacks. In Koyejo, S.; Mohamed, S.; Agarwal, A.; Belgrave, D.; Cho, K.; and Oh, A., eds., *Advances in Neural Information Processing Systems*, volume 35, 7546–7560. Curran Associates, Inc.
- Zagoruyko, S.; and Komodakis, N. 2016. Wide Residual Networks. In Richard C. Wilson, E. R. H.; and Smith, W. A. P., eds., *Proceedings of the British Machine Vision Conference (BMVC)*, 87.1–87.12. BMVA Press. ISBN 1-901725-59-6.
- Zhang, F.; Chowdhury, S. P.; and Christakis, M. 2020. DeepSearch: a simple and effective blackbox attack for deep neural networks. In *Proceedings of the 28th ACM Joint Meeting on European Software Engineering Conference and Symposium on the Foundations of Software Engineering, ESEC/FSE 2020*, 800–812. New York, NY, USA: Association for Computing Machinery. ISBN 9781450370431.
- Zhang, R.; Isola, P.; Efros, A. A.; Shechtman, E.; and Wang, O. 2018. The Unreasonable Effectiveness of Deep Features as a Perceptual Metric. In *2018 IEEE/CVF Conference on Computer Vision and Pattern Recognition*, 586–595.
- Zhang, Y.; Xie, F.; and Chen, J. 2023. TFormer: A throughout fusion transformer for multi-modal skin lesion diagnosis. *Comput. Biol. Med.*, 157(C).
- Zhao, S.; Li, T.; Zhang, B.; Zhai, Y.; Liu, Z.; and Han, Y. 2024. Improving Transferability of Adversarial Examples with Adversaries Competition. In *2024 IEEE International Conference on Multimedia and Expo (ICME)*, 1–6.
- Zhao, Z.; Dua, D.; and Singh, S. 2018. Generating Natural Adversarial Examples. In *International Conference on Learning Representations*.
- Zhao, Z.; Liu, Z.; and Larson, M. 2020. Towards Large Yet Imperceptible Adversarial Image Perturbations With Perceptual Color Distance. In *2020 IEEE/CVF Conference on Computer Vision and Pattern Recognition (CVPR)*, 1036–1045.
- Zhong, Y.; and Deng, W. 2021. Towards Transferable Adversarial Attack Against Deep Face Recognition. *IEEE Transactions on Information Forensics and Security*, 16: 1452–1466.
- Zhou, F.; Ling, H.; Shi, Y.; Chen, J.; Li, Z.; and Li, P. 2024. Improving the Transferability of Adversarial Attacks on Face Recognition With Beneficial Perturbation Feature Augmentation. *IEEE Transactions on Computational Social Systems*, 11(6): 8130–8142.
- Zhou, Z.; Shao, S.; Bai, L.; Xu, Z.; Han, B.; and Xie, Z. 2025. Golden Noise for Diffusion Models: A Learning Framework. arXiv:2411.09502.

Reproducibility Checklist

This paper:

- Includes a conceptual outline and/or pseudocode description of AI methods introduced **yes**
 - Clearly delineates statements that are opinions, hypothesis, and speculation from objective facts and results **yes**
 - Provides well marked pedagogical references for less-familiar readers to gain background necessary to replicate the paper **yes**
1. Does this paper make theoretical contributions? **yes**
If yes, please complete the list below.
 - All assumptions and restrictions are stated clearly and formally. **yes**
 - All novel claims are stated formally (e.g., in theorem statements). **yes**
 - Proofs of all novel claims are included. **yes**
 - Proof sketches or intuitions are given for complex and/or novel results. **yes**
 - Appropriate citations to theoretical tools used are given. **yes**
 - All theoretical claims are demonstrated empirically to hold. **yes**
 - All experimental code used to eliminate or disprove claims is included. **NA**
 2. Does this paper rely on one or more datasets? **yes**
If yes, please complete the list below.
 - A motivation is given for why the experiments are conducted on the selected datasets **yes**
 - All novel datasets introduced in this paper are included in a data appendix. **NA**
 - All novel datasets introduced in this paper will be made publicly available upon publication of the paper with a license that allows free usage for research purposes. **NA**
 - All datasets drawn from the existing literature (potentially including authors' own previously published work) are accompanied by appropriate citations. **yes**
 - All datasets drawn from the existing literature (potentially including authors' own previously published work) are publicly available. **yes**
 - All datasets that are not publicly available are described in detail, with explanation why publicly available alternatives are not scientifically satisfying. **NA**
 3. Does this paper include computational experiments? **yes**
If yes, please complete the list below.
 - Any code required for pre-processing data is included in the appendix. **no**
 - All source code required for conducting and analyzing the experiments is included in a code appendix. **no**
 - All source code required for conducting and analyzing the experiments will be made publicly available upon publication of the paper with a license that allows free usage for research purposes. **yes**
- All source code implementing new methods have comments detailing the implementation, with references to the paper where each step comes from **yes**
 - If an algorithm depends on randomness, then the method used for setting seeds is described in a way sufficient to allow replication of results. **yes**
 - This paper specifies the computing infrastructure used for running experiments (hardware and software), including GPU/CPU models; amount of memory; operating system; names and versions of relevant software libraries and frameworks. **yes**
 - This paper formally describes evaluation metrics used and explains the motivation for choosing these metrics. **yes**
 - This paper states the number of algorithm runs used to compute each reported result. **yes**
 - Analysis of experiments goes beyond single-dimensional summaries of performance (e.g., average; median) to include measures of variation, confidence, or other distributional information. **yes**
 - The significance of any improvement or decrease in performance is judged using appropriate statistical tests (e.g., Wilcoxon signed-rank). **yes**
 - This paper lists all final (hyper-)parameters used for each model/algorithm in the paper's experiments. **yes**
 - This paper states the number and range of values tried per (hyper-) parameter during development of the paper, along with the criterion used for selecting the final parameter setting. **yes**

Supplementary Material

Theoretical Derivation

Derivation of equation (8)

According to the Bayes's theorem $P(AB) = P(A)P(B|A)$ and $P(ABC) = P(A)P(B|A)P(C|AB)$, we want to sample $\tilde{\mathbf{x}}_{t-1}$ based on $\bar{\mathbf{x}}_{t-1}$ following the equation.

$$\begin{aligned}
 & p_\theta(\tilde{\mathbf{x}}_{t-1}|\bar{\mathbf{x}}_{t-1}, y_{tar}) \\
 = & \frac{p_\theta(\tilde{\mathbf{x}}_{t-1}, \bar{\mathbf{x}}_{t-1}, y_{tar})}{p_\theta(\bar{\mathbf{x}}_{t-1}, y_{tar})} \\
 = & \frac{p_\theta(y_{tar}|\tilde{\mathbf{x}}_{t-1}, \bar{\mathbf{x}}_{t-1}) \cdot p_\theta(\tilde{\mathbf{x}}_{t-1}|\bar{\mathbf{x}}_{t-1}) \cdot p_\theta(\bar{\mathbf{x}}_{t-1})}{p_\theta(y_{tar}|\bar{\mathbf{x}}_{t-1}) \cdot p_\theta(\bar{\mathbf{x}}_{t-1})} \\
 = & \frac{p_\theta(y_{tar}|\tilde{\mathbf{x}}_{t-1}, \bar{\mathbf{x}}_{t-1}) \cdot p_\theta(\tilde{\mathbf{x}}_{t-1}|\bar{\mathbf{x}}_{t-1})}{p_\theta(y_{tar}|\bar{\mathbf{x}}_{t-1})} \\
 = & \frac{p_\theta(y_{tar}, \tilde{\mathbf{x}}_{t-1}, \bar{\mathbf{x}}_{t-1})}{p_\theta(\tilde{\mathbf{x}}_{t-1}, \bar{\mathbf{x}}_{t-1})} \cdot \frac{p_\theta(\tilde{\mathbf{x}}_{t-1}|\bar{\mathbf{x}}_{t-1})}{p_\theta(y_{tar}|\bar{\mathbf{x}}_{t-1})} \\
 = & \frac{p_\theta(\tilde{\mathbf{x}}_{t-1}|\bar{\mathbf{x}}_{t-1}, y_{tar}) \cdot p_\theta(y_{tar}|\tilde{\mathbf{x}}_{t-1})}{p_\theta(\bar{\mathbf{x}}_{t-1}|\tilde{\mathbf{x}}_{t-1})} \cdot \frac{p_\theta(\tilde{\mathbf{x}}_{t-1}|\bar{\mathbf{x}}_{t-1})}{p_\theta(y_{tar}|\bar{\mathbf{x}}_{t-1})} \quad (17)
 \end{aligned}$$

Owing to the Markov property of the forward process, we have $p_\theta(\tilde{\mathbf{x}}_{t-1}|\bar{\mathbf{x}}_{t-1}, y_{tar}) = p_\theta(\tilde{\mathbf{x}}_{t-1}|\bar{\mathbf{x}}_{t-1})$. Thus equation (17) can be simplified to:

$$p_\theta(\tilde{\mathbf{x}}_{t-1}|\bar{\mathbf{x}}_{t-1}, y_{tar}) = \frac{p_\theta(\tilde{\mathbf{x}}_{t-1}|\bar{\mathbf{x}}_{t-1}) \cdot p_\theta(y_{tar}|\tilde{\mathbf{x}}_{t-1})}{p_\theta(y_{tar}|\bar{\mathbf{x}}_{t-1})} \quad (18)$$

We express it in exponential form.

$$\begin{aligned}
 & p_\theta(\tilde{\mathbf{x}}_{t-1}|\bar{\mathbf{x}}_{t-1}, y_{tar}) \\
 = & p_\theta(\tilde{\mathbf{x}}_{t-1}|\bar{\mathbf{x}}_{t-1}) \cdot e^{\log p_\theta(y_{tar}|\tilde{\mathbf{x}}_{t-1}) - \log p_\theta(y_{tar}|\bar{\mathbf{x}}_{t-1})} \quad (19)
 \end{aligned}$$

We perform a Taylor expansion of $\log p_\theta(y_{tar}|\tilde{\mathbf{x}}_{t-1})$ around the mean of the sampling distribution, denoted as $\tilde{\mathbf{x}}_{t-1} = \mu(\bar{\mathbf{x}}_{t-1})$, where μ represents the predicted mean of the Gaussian noise during the inference process (denote $\mu(\bar{\mathbf{x}}_{t-1})$ as $\boldsymbol{\mu}$ for concise).

$$\begin{aligned}
 & \log p_\theta(y_{tar}|\tilde{\mathbf{x}}_{t-1}) \\
 \approx & \log p_\theta(y_{tar}|\boldsymbol{\mu}) + (\tilde{\mathbf{x}}_{t-1} - \boldsymbol{\mu})^T [\nabla_{\boldsymbol{\mu}} \log p_\theta(y_{tar}|\boldsymbol{\mu})] \\
 = & (\tilde{\mathbf{x}}_{t-1} - \boldsymbol{\mu})^T \mathbf{g} + C_1 \quad (20)
 \end{aligned}$$

where $\mathbf{g} = \nabla_{\boldsymbol{\mu}} \log p_\theta(y_{tar}|\boldsymbol{\mu})$, C_1 is a constant.

Assume logarithmic probability density function of $p_\theta(\tilde{\mathbf{x}}_{t-1}|\bar{\mathbf{x}}_{t-1})$ is given by:

$$\log p_\theta(\tilde{\mathbf{x}}_{t-1}|\bar{\mathbf{x}}_{t-1}) = -\frac{1}{2} (\tilde{\mathbf{x}}_{t-1} - \boldsymbol{\mu})^T \boldsymbol{\sigma}_t^{-1} (\tilde{\mathbf{x}}_{t-1} - \boldsymbol{\mu}) \quad (21)$$

Substituting it into the equation (19) and (20) yields:

$$\begin{aligned}
 & \log p_\theta(\tilde{\mathbf{x}}_{t-1}|\bar{\mathbf{x}}_{t-1}, y_{tar}) \\
 \approx & -\frac{1}{2} (\tilde{\mathbf{x}}_{t-1} - \boldsymbol{\mu})^T \boldsymbol{\sigma}_t^{-1} (\tilde{\mathbf{x}}_{t-1} - \boldsymbol{\mu}) + (\tilde{\mathbf{x}}_{t-1} - \boldsymbol{\mu})^T \mathbf{g} \\
 = & -\frac{1}{2} \left[(\tilde{\mathbf{x}}_{t-1} - \boldsymbol{\mu})^T \boldsymbol{\sigma}_t^{-1} (\tilde{\mathbf{x}}_{t-1} - \boldsymbol{\mu}) - 2 (\tilde{\mathbf{x}}_{t-1} - \boldsymbol{\mu})^T \mathbf{g} \right] \\
 = & -\frac{1}{2} \left[(\tilde{\mathbf{x}}_{t-1} - (\boldsymbol{\mu} + \boldsymbol{\sigma}_t \mathbf{g}))^T \boldsymbol{\sigma}_t^{-1} (\tilde{\mathbf{x}}_{t-1} - (\boldsymbol{\mu} + \boldsymbol{\sigma}_t \mathbf{g})) \right] + C \\
 = & \log p(\mathbf{z}), \mathbf{z} \sim \mathcal{N}(\boldsymbol{\mu} + \boldsymbol{\sigma}_t \mathbf{g}, \boldsymbol{\sigma}_t) \quad (22)
 \end{aligned}$$

Thus, sampling with equation (22) should be:

$$\tilde{\mathbf{x}}_{t-1} = \bar{\mathbf{x}}_{t-1} + s_a \boldsymbol{\sigma}_t^2 \mathbf{g} \quad (23)$$

Derivation of equation (9)

The sampling formula for image recognition tasks is similar to that used in image classification tasks, with the primary difference being the replacement of the classification model's gradient, $\nabla_{\tilde{\mathbf{x}}_{t-1}} \log p_f(y_{tar}|\tilde{\mathbf{x}}_{t-1})$, with the recognition model's gradient, $\nabla_{\hat{\mathbf{x}}_0} \log p_f(\mathbf{x}_{tar}|\hat{\mathbf{x}}_0)$. All other theoretical derivations remain unchanged.

Derivation of equation (15)

The derivation of equation (15) is similar to that of equation (8). We perform Taylor expansion around $\mathbf{x}_0 = \mathbf{x}_T$.

$$\begin{aligned}
 & \log p_\theta(y_{tar}|\mathbf{x}_T) \\
 \approx & \log p_\theta(y_{tar}|\mathbf{x}_0) + (\mathbf{x}_T - \mathbf{x}_0)^T [\nabla_{\mathbf{x}_0} \log p_\theta(y_{tar}|\mathbf{x}_0)] \quad (24)
 \end{aligned}$$

From \mathbf{x}_0 to \mathbf{x}_T , we employ the forward process of the diffusion model for sampling.

$$p(\mathbf{x}_T|\mathbf{x}_0) = \mathcal{N}(\mathbf{x}_T; \sqrt{\bar{\alpha}_T} \mathbf{x}_0, (1 - \bar{\alpha}_T) \mathbf{I}) \quad (25)$$

Thus, the noise optimization process is as follows:

$$\mathbf{x}_T = (\sqrt{\bar{\alpha}_T} \mathbf{x}_0 + \sqrt{1 - \bar{\alpha}_T} \boldsymbol{\epsilon}) + \bar{\sigma}_T^2 s_a \nabla_{\mathbf{x}_0} \log p_f(y_{tar}|\mathbf{x}_0) \quad (26)$$

Attack Performance on Recognition Systems

Table 4 presents the attack performance of various methods on the recognition model. We select IR152 (He et al. 2016), FaceNet (Schroff, Kalenichenko, and Philbin 2015), and MobileFace (Chen et al. 2018) as the target recognition model. Our proposed method, ScoreAdv, achieves SOTA performance, surpassing previous approaches such as DI (Xie et al. 2019), VMI (Wang and He 2021), SSA (Long et al. 2022), DFANet (Zhong and Deng 2021), SIA (Wang, Zhang, and Zhang 2023), BSR (Wang et al. 2024), and BPFa (Zhou et al. 2024). As shown in the table, ScoreAdv significantly outperforms other methods in black-box scenarios and achieves competitive or superior results in most white-box settings. This demonstrates that our method is not only effective in attacking image classification models but also exhibits strong performance when targeting recognition models.

Table 4: Attack performance comparison of various methods on image recognition models. We report ASR (%) and transferability. S. represents the surrogate model, while T. represents the target model. In cases where the surrogate model and the target model are identical, the scenario is classified as a white-box attack, with the background highlighted in gray for clarity. The best result is **bolded** and the second best result is underlined.

S.	T.	Attacks	LFW			CebebA-HQ		
			IR152	FaceNet	MobileFace	IR152	FaceNet	MobileFace
IR152		DI	<u>95.4</u>	21.7	14.4	<u>87.9</u>	<u>27.6</u>	27.0
		VMI	92.7	23.9	18.7	92.2	26.4	27.7
		SSA	78.8	21.9	<u>24.0</u>	83.8	23.3	<u>30.7</u>
		DFANet	98.9	15.5	<u>12.5</u>	98.9	21.5	<u>22.4</u>
		SIA	81.7	<u>26.3</u>	19.6	78.4	26.9	30.4
		BSR	52.4	14.7	7.3	48.5	17.3	15.0
		BPFA	92.6	12.9	9.2	90.4	15.8	16.4
		ScoreAdv	98.9	83.9	97.5	<u>95.0</u>	55.0	84.0
FaceNet		DI	18.6	99.8	18.5	22.8	<u>99.4</u>	22.9
		VMI	24.4	99.8	20.7	26.4	99.3	25.7
		SSA	21.6	97.5	<u>30.8</u>	23.5	96.9	<u>36.1</u>
		DFANet	12.1	99.8	11.7	15.2	99.1	19.7
		SIA	<u>29.1</u>	<u>99.5</u>	26.2	29.3	<u>99.4</u>	35.7
		BSR	28.6	98.6	25.9	<u>27.8</u>	98.8	34.0
		BPFA	17.3	98.6	14.7	20.0	99.0	21.7
		ScoreAdv	79.7	98.9	89.4	35.8	99.8	61.9
MobileFace		DI	<u>18.4</u>	<u>32.9</u>	<u>99.2</u>	25.0	<u>32.0</u>	<u>95.2</u>
		VMI	13.6	20.2	<u>99.7</u>	20.2	19.6	98.2
		SSA	13.8	19.6	98.3	22.0	21.0	93.3
		DFANet	7.0	11.9	99.6	10.7	12.6	<u>99.1</u>
		SIA	15.7	26.7	98.4	<u>25.4</u>	25.9	96.3
		BSR	5.4	9.5	84.9	10.8	11.9	77.6
		BPFA	15.8	17.8	97.7	20.7	17.5	96.2
		ScoreAdv	84.9	81.5	100.0	48.1	40.0	100.0

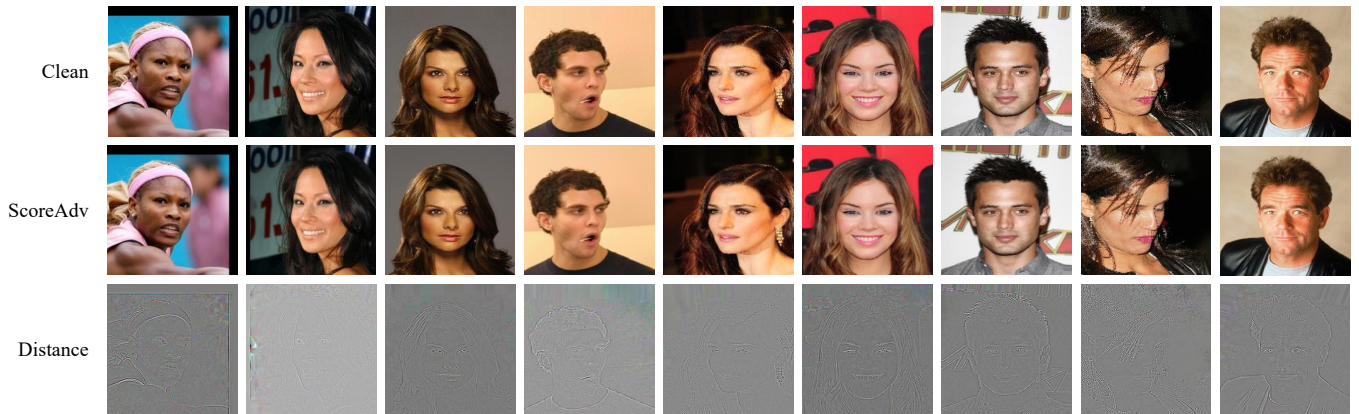


Figure 6: Visualization of adversarial images and perturbations generated by different attack methods. The upper row displays the adversarial images, while the lower row illustrates the corresponding perturbations.

Additional Results

Comparison With More SOTA Methods

While we have already compared our method with the most advanced diffusion-based UAE approaches, we further ex-

tend our evaluation to include additional SOTA methods, such as TI-FGSM (Dong et al. 2019) VENOM (Kuurila-Zhang, Chen, and Zhao 2025), AdvAD (Li et al. 2024), and NatADiff (Collins et al. 2025). As shown in Table 5, Score-

Adv consistently achieves superior performance in both attack success rate and image quality. Moreover, although comparing ScoreAdv with ensemble-based attacks is inherently disadvantageous to us, we still include such comparisons. The results demonstrate that our method remains highly competitive against a wide range of baselines.

Table 5: Comparison with additional SOTA methods and ensemble attacks. The evaluation metrics remain consistent with the main paper. STDMI-F refers to S^2I -TI-DI-MI-FGSM. The best result is **bolded** and the second best result is underlined.

Attacks	Res50	Inc-v3	ViT-B	Mix-B	SSIM
TI-FGSM	94.8	32.5	<u>25.9</u>	<u>48.8</u>	0.716
NatADiff	96.2	18.7	6.6	—	—
AdvAD	98.6	37.6	14.1	31.7	0.887
VENOM	97.5	<u>45.8</u>	17.2	36.0	0.715
ScoreAdv	<u>97.6</u>	46.7	40.1	65.3	<u>0.832</u>
STDMI-F	99.7	51.3	44.8	64.3	0.682

Ablation Study on Saliency Map

As shown in Table 6, we compare the proposed ScoreCAM with other interpretability-based saliency methods, including GradCAM (Selvaraju et al. 2017), and GradCAM++ (Chattopadhyay et al. 2018). Experimental results demonstrate that our approach consistently outperforms the others in both attack effectiveness and image quality.

Table 6: Ablation study on different saliency maps. The best result is **bolded** and the second best result is underlined.

Saliency maps	Res50	Inc-v3	Mix-B	FID
GradCAM	92.6	43.1	63.0	56.758
GradCAM++	93.1	43.5	62.8	54.629
ScoreAdv	97.6	46.7	65.3	44.932